Bioconjugate Chemistry

Communication

Cite This: Bioconjugate Chem. 2018, 29, 1834−1840

pubs.acs.org/bc

Thio-Linked UDP−Peptide Conjugates as O-GlcNAc Transferase Inhibitors

Karim Rafie, Andrii Gorelik, Riccardo Trapannone,† Vladimir S. Borodkin,* and Daan M. F. van Aalten*

Division of Gene Regulation and Expression, School of Life Sciences, University of Dundee, DD1 5EH Dundee, U.K.

Supporting Information

ABSTRACT: O-GlcNAc transferase (OGT) is an essential glycosyltransferase that installs the O-GlcNAc post-translational modification on the nucleocytoplasmic proteome. We report the development of S-linked UDP−peptide conjugates as potent bisubstrate OGT inhibitors. These compounds were assembled in a modular fashion by photoinitiated thiol−ene conjugation of allyl-UDP and optimal acceptor peptides in which the acceptor serine was replaced with cysteine. The conjugate VTPVC(S-propyl-UDP)TA (K_i = 1.3 μM) inhibits the OGT activity in HeLa cell lysates. Linear fusions of this conjugate with cell penetrating peptides were explored as prototypes of cell-penetrant OGT inhibitors. A crystal structure of human OGT with the inhibitor revealed mimicry of the interactions seen in the pseudo-Michaelis complex. Furthermore, a fluorophore-tagged derivative of the inhibitor works as a high affinity probe in a fluorescence polarimetry hOGT assay.

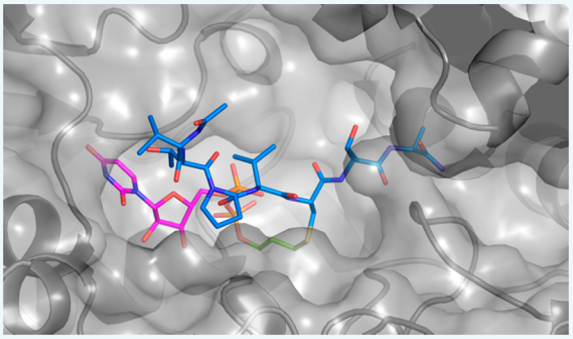

The reversible attachment of β-N-acetylglucosamine (O-GlcNAc) to serine and threonine residues of nucleocytoplasmic proteins is a highly conserved and dynamic post-translational modification (PTM) found in higher eukaryotes.[1,2] The transfer of O-GlcNAc from the donor substrate UDP-GlcNAc onto substrate proteins is catalyzed by the O-GlcNAc transferase (OGT), while the removal is catalyzed by the O-GlcNAc hydrolase (OGA).[3] Both enzymes possess substantial substrate promiscuity, which enables this single pair of enzymes to control the O-GlcNAc proteome linked to the regulation of a range of cellular processes.[4,5] Protein O-GlcNAcylation is essential for proper development of the animal embryo,[6−8] and mutations in the O-GlcNAc transferase have recently been associated with intellectual disability.[9−11] Multiple metabolic pathologies, such as diabetes[12,13] and cancer,[14−16] as well as neurological diseases[17,18] such as Alzheimer's and Parkinson's have been linked to dysregulation of protein O-GlcNAcylation.

Elucidation of the precise biological role(s) of protein O-GlcNAcylation is markedly hampered by the lack of potent and selective inhibitors of OGT.[19] The unusual catalytic machinery of the enzyme, which only seems to be fully assembled on the binding of the donor substrate,[20] has proven to be difficult to target. Previously, high-throughput compound screening studies have yielded cell penetrant small molecules like BZX[21,22] and OSMI1.[23] The former renders OGT inactive by cross-linking Lys^{842} and Cys^{917} in the active site. Given its reactivity, BZX may also target enzymes that contain similar Lys/Cys pairs. OSMI1 inhibits OGT through an as of yet unknown mechanism and was also shown to affect cell surface glycosylation.[23] The most widely used OGT inhibitor, the peracetylated derivative of 5-thio-*N*-acetylglucosamine, hijacks the hexosamine biosynthetic pathway to yield the donor substrate analogue UDP-5S-GlcNAc that is inherently nonselective in the context of several other families of essential UDP-GlcNAc processing glycosyl transferases present in the cell.[24]

Recently, we have reported the synthesis and kinetic evaluation of bisubstrate OGT inhibitors that have been conceived by tethering the anchoring UDP moiety of the donor substrate to the serine side chain of a series of heptapeptides derived from several human OGT (hOGT) acceptor proteins.[25] The bisubstrate UDP−peptide conjugate VTPVS-(O-propyl-UDP)TA **1** acted as a competitive hOGT inhibitor *in vitro* (IC_{50} = 18 μM[25]).

To develop these UDP−peptide conjugates into useful chemical biology tools two problems need to be addressed. First, the potency needs to be increased to effectively compete with the donor substrate UDP-GlcNAc (K_d = 16 μM[20]). Second, the intrinsic cell penetrance of these conjugates is limited by their size and the negative charge of the UDP moiety. To address the first problem, an expedient access to a diverse set of bisubstrate inhibitors was required to enable efficient structure−activity studies. To improve cell penetrance, we aimed to fuse the bisubstrate "warhead" to a selection of cell penetrating peptides (CPP) to achieve cellular uptake.

In our original approach, the phosphorylated "stretched serine" building block was incorporated into the backbone of a

Received: March 16, 2018
Revised: April 30, 2018
Published: May 3, 2018

DOI: 10.1021/acs.bioconjchem.8b00194
Bioconjugate Chem. 2018, 29, 1834−1840

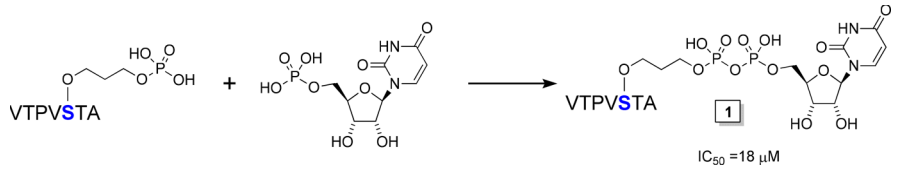

Figure 1. Synthesis and structure of the O-linked UDP−peptide conjugate **1**.[25]

peptide with subsequent formation of the pyrophosphate bond in a reaction with an activated UMP derivative (Figure 1). To improve synthetic efficiency we sought an alternative modular strategy that would enable installation of tethered UDP as the single moiety on a variety of peptide backbones. Advantageously, the suggested convergent approach would also facilitate the assembly of the proposed CPP-bisubstrate inhibitors by solid phase peptide synthesis (SPPS) followed by attachment of the tethered UDP as the last synthetic step.

As the chemical structure of the O-linked UDP−peptide conjugates showed limited opportunity for modular assembly, we instead opted to explore novel S-linked UDP−peptide conjugates that could be accessed by chemoselective cysteine modification with a thiol-reactive tethered UDP derivative (Figure 2). Evaluation of three mainstay techniques for

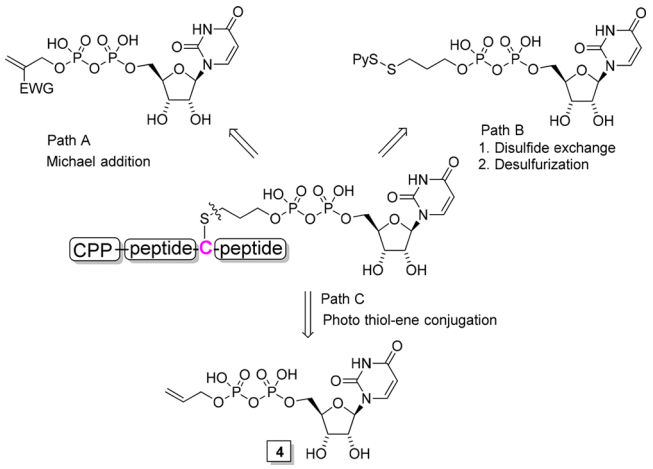

Figure 2. Selected possible approaches to the synthesis of S-linked UDP−peptide conjugates. In path A an electron withdrawing group in the Michael acceptor would disrupt the topological integrity of the linker. Path B leads to isomerization at Cys.[26] Path C allows for the efficient construction of the target molecule.

carbon−sulfur bond formation such as Michael addition (Path A), phosphine promoted disulfide contraction[26] (Path B), and "click" thiol−ene conjugation (TEC)[27−30] (Path C) in the context of construction of such thiol reactive UDP derivatives revealed inherent limitations of the first two approaches (Figure 2). Indeed, introduction of a mandatory electron withdrawing group would disrupt the topological integrity of the linker in the proposed Michael type reactive derivative. In turn, disulfide contraction, widely used for preparation of S-linked glycoproteins, seemed to be less attractive for peptide substrates, as it would unavoidably result in the loss of the stereochemical integrity of the linking cysteine. In fact, only photoinitiated TEC reaction of cysteine containing peptides with simplistic allyl-UDP **4** held promise for an efficient assembly of the envisaged conjugates.

To synthesize the requisite allyl-UDP **4** the Bogachev−Kiessling[31,32] protocol was used by coupling UMP *N*-methyl imidazolide **3** with the crude bis-triethylammonium salt of allyl phosphoric acid, prepared in turn from allyl bis-fluorenemethyl phosphate **2** (Scheme 1, Scheme S8).

The structure of **4** was unambiguously assigned by a set of spectroscopic methods (Figures S1−S3); the presence of a pyrophosphate bond was confirmed by a typical pair of doublets (σ −11, −12, $J_{P,P}$ = 21 Hz) in the ^{31}P NMR spectrum. The photoinitiated TEC reaction between **4** and 20% molar excess of the substrate peptide VTPVCTA **5** was initially attempted at 10 mM in 0.1 M acetate buffer (pH 4) in the presence of 20% of different water-soluble photoinitiators VA-044, DMPA (50% MeOH additive), or LAP.[33] The reactions were irradiated using an 8 W Camag TLC reader lamp at 366 nm and monitored by LC-MS. We found that LAP efficiently mediated the conjugation, resulting in clean formation of the expected product **6** (*m*/*z* 1175) after only 10 min (Scheme 2A).

On the other hand, <5% conversion was detected with VA-044, while no reaction took place with DMPA. The TEC reaction was equally efficient when no excess of the substrate peptide was present and with only 10% of the photoinitiator. No products were observed in the absence of LAP or without UV light. The reaction was scaled up to 0.05 mmol (20 mM in water), and the S-linked UDP−peptide conjugate **6** was isolated by preparative HPLC in 56% yield. The structure of the product was verified by ^{1}H and ^{13}C NMR spectra, proving the presence of the peptide backbone and the UDP moiety (Figures S4, S5). The ^{31}P spectrum showed two broadened

Scheme 1. Chemical Synthesis of Allyl-UDP[a]

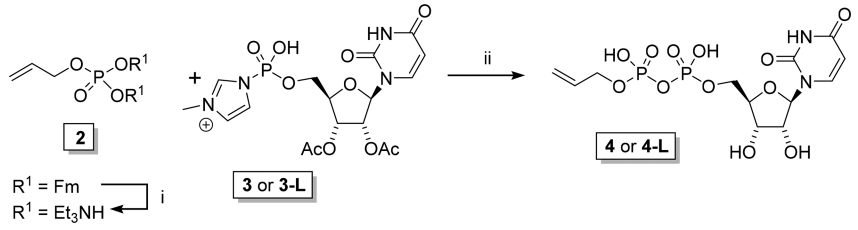

[a](i) Et_3N-DCM, 4:1, 16 h; (ii) a) Bogachev−Kiessling coupling, 3 h; b) MeOH, Et_3N, H_2O, 16 h, 44%.

DOI: 10.1021/acs.bioconjchem.8b00194
Bioconjugate Chem. 2018, 29, 1834−1840

Scheme 2. Photoinitiated Thiol−Ene Conjugation of Cysteine Containing Peptides with Allyl-UDP[a]

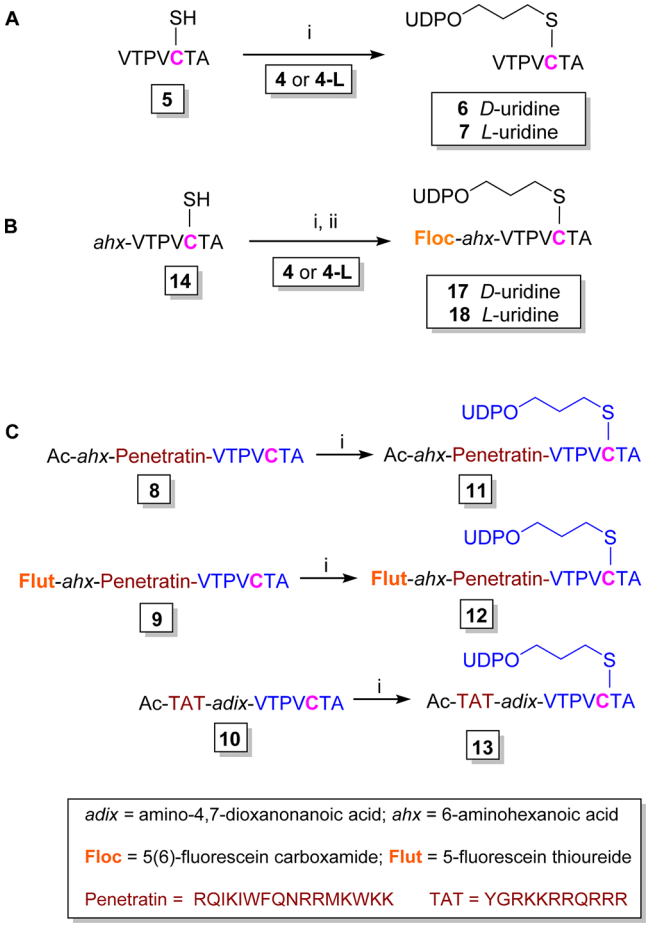

[a](i) 8 W 366 nm, 10 min, 50−55%; (ii) 5(6)-fluorescein NHS ester, DMF, 0.15 M $NaHCO_3$, 3 h, 85%.

singlets at σ −10.94 and −11.48, confirming the integrity of the pyrophosphate bond.

The inhibitory potency of **6** was assessed by the previously described fluorometric OGT activity assay.[25] Unexpectedly, the S-linked UDP peptide conjugate **6** appeared to be an almost 10-fold more potent hOGT inhibitor (IC_{50} = 2 μM) than its O-linked progenitor **1**[25] (Figure 3A). To provide a negative control and on the assumption that hOGT evolved to bind *D*-configured UDP, we synthesized the *L*-uridine congener **7** starting from allyl-*L*-UDP **4-L** (Scheme 2A, Scheme S10), which showed no inhibition of hOGT (Figure 3A). Next, we demonstrated that **6** is also a hOGT inhibitor in a cell-free system, reducing protein O-GlcNAcylation in a dose-dependent manner by about 50% at 1 mM (Figure 3B, Figure S6).

Next, we attempted the assembly of the potentially cell penetrating bisubstrate hOGT inhibitors. To this end, starting from peptides featuring a VTPVCTA C-terminus and either Penetratin (RQIKIWFQNRRMKWKK - **8**/**9**)[34] or TAT (YGRKKRRQRRR - **10**)[35] peptides at the N-terminus, we synthesized S-linked UDP peptide conjugates **11**−**13** by TEC reaction with allyl-UDP **4** (Scheme 2C).

Encouragingly, the conjugates **11** and **13** (IC_{50}[**13**] = 5 μM, Figure S7) were shown to be almost as potent hOGT inhibitors *in vitro* as the parent compound **6**. However, neither **11** nor **13** had a noticeable effect on total O-GlcNAcylation in cell cultures at concentrations up to 1 mM (Figure S8). Moreover, microscopy of the HeLa cells treated with the 5-fluorescein thioureide (Flut) labeled conjugate **12** for 24 h revealed fluorescent puncta (Figure S8). Taken together, these data suggest that while **12** and, implicitly **11** and **13**, could cross the cell membrane, they remain trapped in the early endosomes[36,37] and therefore cannot target cytosolic hOGT.

Discovery of the potent hOGT binder **6** also offers an opportunity for development of a sensitive hOGT fluorescence polarimetry assay (FP). We explored the fluorescently tagged derivative **17** of the inhibitor as a high affinity FP probe. To this end, the peptide **14** was efficiently transformed into corresponding S-linked UDP−peptide conjugate by TEC reaction with allyl-UDP **4**. Next, the N-terminal 6-aminohexanoyl (*ahx*) residue was tagged with 5(6)-fluorescein NHS ester to give the requisite 5(6)-fluorescein carboxamide (Floc) labeled derivative **17** (Scheme 2B). The same reaction

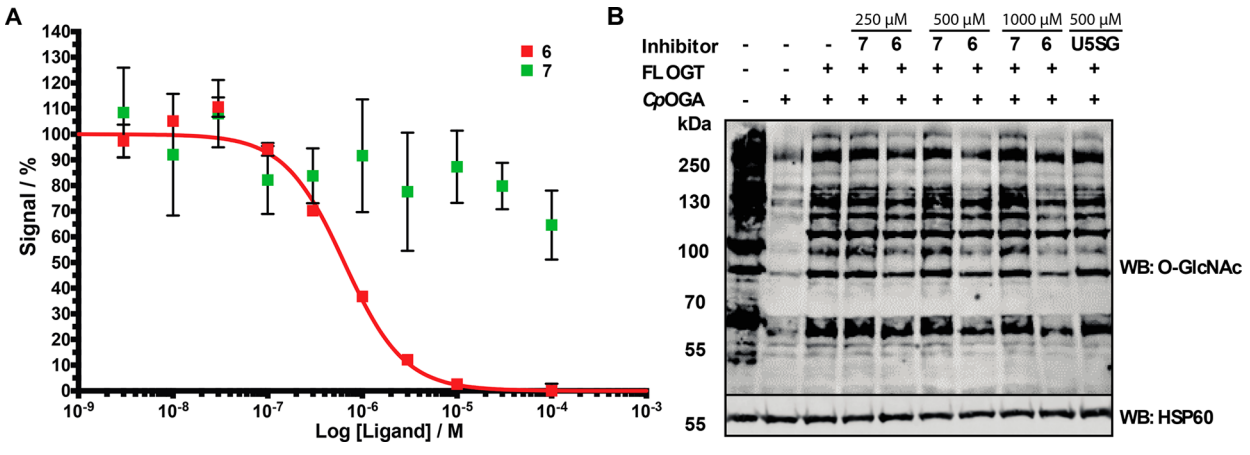

Figure 3. (A) Dose−response curves of inhibition of hOGT activity in the presence of increasing concentrations of **6** and **7**. Errors shown represent the s.e.m. of three replicates. (B) Western blot analysis of cell lysate in the presence and absence of **6**, **7**, and UDP-5S-GlcNAc. HeLa cell lysates were O-GlcNAc stripped by the potent bacterial O-GlcNAcase *Cp*OGA, whose activity was then blocked by the potent OGA inhibitor GlcNAcstatin G. These stripped lysates were then re-O-GlcNAcylated by recombinant OGT and blotted for protein O-GlcNAcylation using the RL2 antibody. HSP60 was used as a loading control.

DOI: 10.1021/acs.bioconjchem.8b00194
Bioconjugate Chem. 2018, 29, 1834−1840

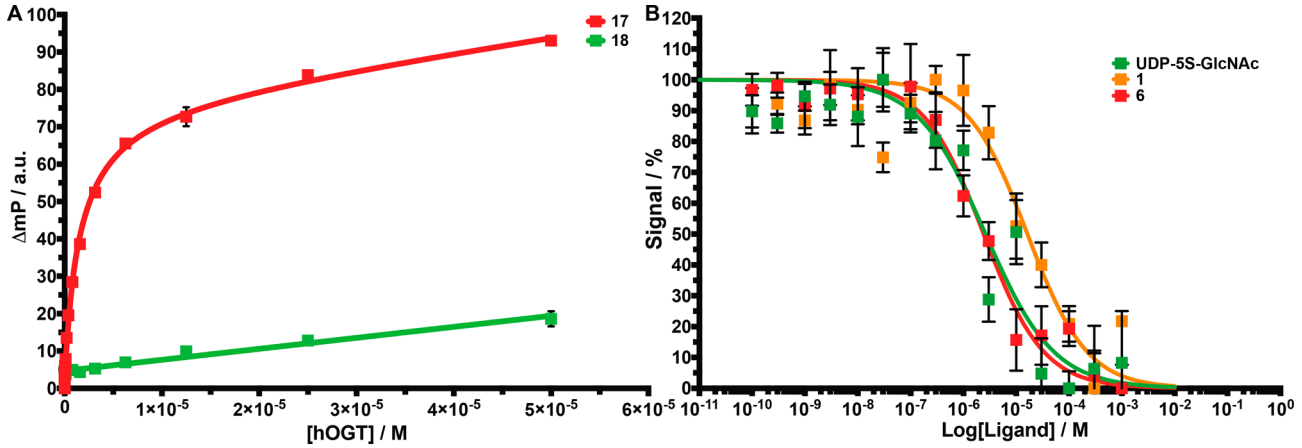

Figure 4. (**A**) FP assay showing the binding of **17** and **18** to hOGT. (**B**) Dose−response curves from the FP assay showing the displacement of **17** by UDP-5S-GlcNAc, **1** and **6**. Errors shown represent the s.e.m. of at least three replicates.

Table 1. Inhibition of hOGT with UDP−Peptide Bisubstrate Conjugates 6 and 29−38

	sequence	origin/Cys position	Cys peptide	product	K_i (μM)
1	VTPVCTA	RB2_7-S5C	**5**	**6**	1.3 ± 0.8
2	VPTVCTA	*pseudo* RB2_7-S5C	**19**	**29**	12.8 ± 4.5
3	SVPYCSA	TAB1_7-S5C	**20**	**30**	2.3 ± 1.6
4	VTPVCSA	CK2_7-S5C	**21**	**31**	1.2 ± 1.3
5	VTPVCRA	SEQ_7-S5C	**22**	**32**	1.3 ± 0.5
6	PVFTCRS	KER_7-S5C	**23**	**33**	12.5 ± 7
7	VTPVCTATH	RB2_9-S5C	**24**	**34**	12.7 ± 2.3
8	SVPYCSAQS	TAB1_9-S5C	**25**	**35**	15 ± 2.3
9	PVFTCRSAA	KER_9-S5C	**26**	**36**	56 ± 32
10	PVCTATHSLSRLH	RB2_13-S3C	**27**	**37**	80 ± 46
11	KENSPAVTPVCTA	RB2_13-S11C	**28**	**38**	1.8 ± 1.3

sequence was performed with **14** and allyl-*L*-UDP **4-L** to give the negative control compound **18**.

Direct binding affinity of compound **17** to hOGT was measured, yielding a K_D of 1.6 μM, whereas no quantifiable binding could be detected for the corresponding negative control **18** (Figure 4A). The observed value is in good agreement with the IC_{50} of 2 μM established in our activity assay.

To verify whether the probe **17** could be used in a workable FP hOGT assay we demonstrated that the available competitive inhibitors UDP-5S-GlcNAc[24] and **1** displace **17** from the complex with the enzyme in a dose-dependent manner (Figure 4B). The derived values of K_i = 7 ± 2 μM (**1**) and K_i = 5 ± 2 μM (UDP-5S-GlcNAc) were in agreement with the previously reported affinities,[20,25] validating this assay.

Next, we used this assay platform to examine the effect of the peptide sequence on the inhibitory potency of the *S*-linked UDP−peptide conjugates. We compiled a set of peptides derived from the known hOGT substrate proteins RB2, TAB1, CK2, and KER, as well as a previously published hOGT sequon[38] (Table 1). The topology of the heptapeptides in the 7-S5C subseries (**19**−**23**) was chosen to replicate that of the peptide **5**. The nonapeptides 9-S5C (**24**−**26**) were designed with a centrally located Cys. The pair of the tridecapeptides **27** and **28** was included to explore distant regions of the binding groove. The TEC reaction of allyl-UDP **4** with all substrates worked routinely well to give an array of the novel *S*-linked UDP−peptide conjugates **29**−**38** (Table 1, Table S1) that were evaluated by the modified FP assay (Table 1, Figure 5).

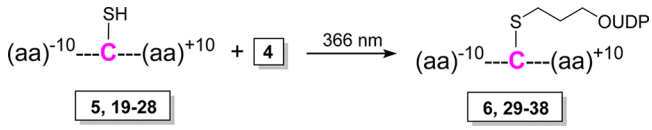

Figure 5. Schematic of the synthesis of UDP−peptide bisubstrate conjugates shown in Table 1.

The collated data (Table 1) suggest that conjugates derived from the heptapeptides 7-S5C cover the minimal structure of the bisubstrate inhibitor until there is proline in the −2 position, as the binding potency remains in the range of 1 ± 0.5 μM (note the potency drop in the conjugate **29** (entry 2)). These data, taken together, are in good agreement with previous findings that emphasize the importance of a proline in the −2 position.[38] Notably, C-terminal elongation of conjugates in 9-S5C and 13-SC3 series results in a steady potency drop, while N-terminal extension did not affect the binding of the 13-S11C conjugate **38**.

To reveal likely reasons for the enhanced potency of the *S*-linked UDP−peptide conjugates we collected high-resolution synchrotron diffraction data of crystals of hOGT in complex with **6** (1.85 Å, R_{work}/R_{free} = 0.22/0.25) or its *O*-linked progenitor **1** (1.68 Å, R_{work}/R_{free} = 0.19/0.22) (Figure 6, Table S2). Structure solution by molecular replacement and subsequent refinement revealed continuous $|F_o|-|F_c|$ electron density for both ligands allowing the unambiguous placement of each (Figure S9). The fully refined models revealed both conjugates bind to the OGT active site in a conformation closely resembling the previously reported pseudo-Michaelis

DOI: 10.1021/acs.bioconjchem.8b00194
Bioconjugate Chem. 2018, 29, 1834−1840

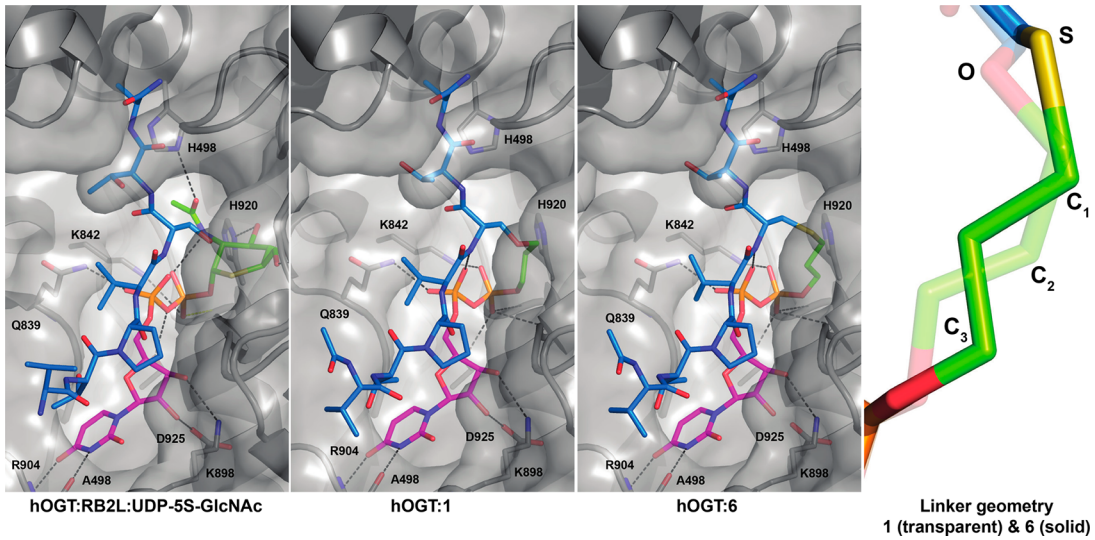

Figure 6. Crystal structures of the pseudo-Michaelis complex (PDB 5C1D[38]) and bisubstrate inhibitors **1** and **6** bound to hOGT. The protein is shown as a grey cartoon overlaid with a grey surface, the peptide part is colored in blue, the linker/sugar is colored in green, and the UDP moiety is colored in magenta.

complex of hOGT with UDP-5S-GlcNAc and an acceptor peptide[20] (Figure 6). The largest atomic shift between the UDP moieties of conjugates **1** and **6** and the corresponding substrates/substrate analogues is 0.7−0.8 Å. Shifts were also observed between the positions of the linking oxygen and sulfur (0.8 Å) and the positions of the linker C_1 atoms (1.1 Å). Overall, in the conjugate **1** the linker adopts a synclinal conformation (dihedral angle $O-C_1-C_2-C_3$ of 72°), while in **6** the linker adopts an antiperiplanar conformation (dihedral angle $S-C_1-C_2-C_3$ 171.4°). This difference may contribute to the increased potency of **6**, as the antiperiplanar conformation of the thio-propyl linker seen in **6** is energetically more favorable than the synclinal conformation of the oxy-propyl linker in **1**.

In conclusion, we developed a modular synthetic approach to S-linked UDP−peptide conjugates using a photoinitiated TEC reaction between allyl-UDP and cysteine containing peptides. A series of conjugates sharing the XXPXC(S-propyl-UDP)XX scaffold showed binding potency toward hOGT in the 1 ± 0.5 μM range *in vitro*, which places them among the most potent hOGT inhibitors reported to date. The increased potency of the conjugate VTPVC(S-propyl-UDP)TA in comparison with its O-linked progenitor correlates with the more relaxed conformation of the thiopropyl linker. We have shown that the chosen S-linked conjugate inhibits recombinant hOGT activity in HeLa cell lysates and successfully assembled two prototypes of the cell-penetrating bisubstrate hOGT inhibitors that feature Penetratin and TAT peptides C-terminally extended with the VPTVC(S-propyl-UDP)TA motif. Finally, we developed a practical variant of the fluorescence polarimetry hOGT assay using a fluorescently labeled derivative of the bisubstrate conjugate as a high affinity probe suitable for high-throughput screening. Further optimization of the structure of the novel hOGT bisubstrate inhibitors as well as evaluating of different types of cell penetrating vehicles could lead to further improvements of this scaffold.

■ ASSOCIATED CONTENT

Supporting Information

The Supporting Information is available free of charge on the ACS Publications website at DOI: 10.1021/acs.bioconjchem.8b00194.

Synthetic procedures and spectral data for all new compounds, methods, figures, and tables (PDF)

Accession Codes

X-ray diffraction data and refined structures have been deposited with the Protein Data Bank under accession codes 5NPS (**1**) and 5NPR (**6**).

■ AUTHOR INFORMATION

Corresponding Authors

*E-mail: vsborodkin@dundee.ac.uk.
*E-mail: dmfvanaalten@dundee.ac.uk.

ORCID

Karim Rafie: 0000-0003-2418-0061
Vladimir S. Borodkin: 0000-0002-8479-3188

Present Address

†Max F. Perutz Laboratories, Vienna Biocenter, University of Vienna, 1030 Vienna, Austria.

Author Contributions

K.R., V.S.B., and D.M.F.v.A. conceived the study. V.S.B. performed chemical synthesis; K.R. performed structural biology, steady-state kinetics, and fluorescence polarimetry experiments; A.G. and R.T. performed Western blot experiments; R.T. performed fluorescence microscopy experiments; K.R., V.S.B., and D.M.F.v.A. interpreted the data; K.R., V.S.B., and D.M.F.v.A. wrote the manuscript with input from all authors.

Notes

The authors declare no competing financial interest.
Additional supporting research validation reports of the deposited structures for this article may be accessed at no charge at http://wwpdb.org/validation/2016/XrayValidationReportHelp.

DOI: 10.1021/acs.bioconjchem.8b00194
Bioconjugate Chem. 2018, 29, 1834−1840

■ ACKNOWLEDGMENTS

We thank the European Synchrotron Radiation Facility (ESRF) for beam time on beamlines ID30A-1 and ID29. This work was funded by a Wellcome Trust Senior Research Fellowship (WT087590MA) to DMFvA.

■ REFERENCES

(1) Torres, C. R., and Hart, G. W. (1984) Topography and polypeptide distribution of terminal N-acetylglucosamine residues on the surfaces of intact lymphoc. *J. Biol. Chem. 259*, 3308−3317.
(2) Hart, G. W., Housley, M. P., and Slawson, C. (2007) Cycling of O-linked beta-N-acetylglucosamine on nucleocytoplasmic proteins. *Nature 446*, 1017−1022.
(3) Dong, D. L., and Hart, G. W. (1994) Purification and characterization of an O-GlcNAc selective N-acetyl-beta-D-glucosaminidase from rat spleen cytosol. *J. Biol. Chem. 269*, 19321−19330.
(4) Hahne, H., Sobotzki, N., Nyberg, T., Helm, D., Borodkin, V. S., van Aalten, D. M., Agnew, B., and Kuster, B. (2013) Proteome wide purification and identification of O-GlcNAc-modified proteins using click chemistry and mass spectrometry. *J. Proteome Res. 12*, 927−936.
(5) Chalkley, R. J., Thalhammer, A., Schoepfer, R., and Burlingame, A. L. (2009) Identification of protein O-GlcNAcylation sites using electron transfer dissociation mass spectrometry on native peptides. *Proc. Natl. Acad. Sci. U. S. A. 106*, 8894−8899.
(6) Webster, D. M., Teo, C. F., Sun, Y., Wloga, D., Gay, S., Klonowski, K. D., Wells, L., and Dougan, S. T. (2009) O-GlcNAc modifications regulate cell survival and epiboly during zebrafish development. *BMC Dev. Biol. 9*, 28.
(7) Watson, L. J., Long, B. W., DeMartino, A. M., Brittian, K. R., Readnower, R. D., Brainard, R. E., Cummins, T. D., Annamalai, L., Hill, B. G., and Jones, S. P. (2014) Cardiomyocyte Ogt is essential for postnatal viability. *Am. J. Physiol Heart Circ Physiol 306*, H142−153.
(8) Gambetta, M. C., Oktaba, K., and Müller, J. (2009) Essential Role of the Glycosyltransferase Sxc/Ogt in Polycomb Repression. *Science 325*, 93−96.
(9) Bouazzi, H., Lesca, G., Trujillo, C., Alwasiyah, M. K., and Munnich, A. (2015) Nonsyndromic X-linked intellectual deficiency in three brothers with a novel MED12 missense mutation [c.5922G > T (p.Glu1974His)]. *Clin Case Rep 3*, 604−609.
(10) Vaidyanathan, K., Niranjan, T., Selvan, N., Teo, C. F., May, M., Patel, S., Weatherly, B., Skinner, C., Opitz, J., Carey, J., et al. (2017) Identification and characterization of a missense mutation in the O-linked beta-N-acetylglucosamine (O-GlcNAc) transferase gene that segregates with X-linked intellectual disability. *J. Biol. Chem. 292*, 8948−8963.
(11) Willems, A. P., Gundogdu, M., Kempers, M. J. E., Giltay, J. C., Pfundt, R., Elferink, M., Loza, B. F., Fuijkschot, J., Ferenbach, A. T., van Gassen, K. L. I., et al. (2017) Mutations in N-acetylglucosamine (O-GlcNAc) transferase in patients with X-linked intellectual disability. *J. Biol. Chem. 292*, 12621−12631.
(12) McLarty, J. L., Marsh, S. A., and Chatham, J. C. (2013) Post-translational protein modification by O-linked N-acetyl-glucosamine: Its role in mediating the adverse effects of diabetes on the heart. *Life Sci. 92*, 621−627.
(13) Banerjee, P. S., Ma, J. F., and Hart, G. W. (2015) Diabetes-associated dysregulation of O-GlcNAcylation in rat cardiac mitochondria. *Proc. Natl. Acad. Sci. U. S. A. 112*, 6050−6055.
(14) Itkonen, H. M., Minner, S., Guldvik, I. J., Sandmann, M. J., Tsourlakis, M. C., Berge, V., Svindland, A., Schlomm, T., and Mills, I. G. (2013) O-GlcNAc Transferase Integrates Metabolic Pathways to Regulate the Stability of c-MYC in Human Prostate Cancer Cells. *Cancer Res. 73*, 5277−5287.
(15) Li, Z. H., and Yi, W. (2014) Regulation of cancer metabolism by O-GlcNAcylation. *Glycoconjugate J. 31*, 185−191.
(16) Singh, J. P., Zhang, K. S., Wu, J., and Yang, X. Y. (2015) O-GlcNAc signaling in cancer metabolism and epigenetics. *Cancer Lett. 356*, 244−250.
(17) Yuzwa, S. A., and Vocadlo, D. J. (2014) O-GlcNAc and neurodegeneration: biochemical mechanisms and potential roles in Alzheimer's disease and beyond. *Chem. Soc. Rev. 43*, 6839−6858.
(18) Foerster, S., Welleford, A. S., Triplett, J. C., Sultana, R., Schmitz, B., and Butterfield, D. A. (2014) Increased O-GlcNAc levels correlate with decreased O-GlcNAcase levels in Alzheimer disease brain. *Biochim. Biophys. Acta, Mol. Basis Dis. 1842*, 1333−1339.
(19) Trapannone, R., Rafie, K., and van Aalten, D. M. F. (2016) O-GlcNAc transferase inhibitors: current tools and future challenges. *Biochem. Soc. Trans. 44*, 88−93.
(20) Schimpl, M., Zheng, X., Borodkin, V. S., Blair, D. E., Ferenbach, A. T., Schuettelkopf, A. W., Navratilova, I., Aristotelous, T., Albarbarawi, O., Robinson, D. A., et al. (2012) O-GlcNAc transferase invokes nucleotide sugar pyrophosphate participation in catalysis. *Nat. Chem. Biol. 8*, 969−974.
(21) Gross, B., Kraybill, B., and Walker, S. (2005) Discovery of O-GlcNAc transferase inhibitors. *J. Am. Chem. Soc. 127*, 14588−14589.
(22) Jiang, J., Lazarus, M. B., Pasquina, L., Sliz, P., and Walker, S. (2012) A neutral diphosphate mimic crosslinks the active site of human O-GlcNAc transferase. *Nat. Chem. Biol. 8*, 72−77.
(23) Ortiz-Meoz, R. F., Jiang, J., Lazarus, M. B., Orman, M., Janetzko, J., Fan, C., Duveau, D. Y., Tan, Z. W., Thomas, C. J., and Walker, S. (2015) A small molecule that inhibits OGT activity in cells. *ACS Chem. Biol. 10*, 1392−1397.
(24) Gloster, T., Zandberg, W., Heinonen, J., Shen, D., Deng, L., and Vocadlo, D. (2011) Hijacking a biosynthetic pathway yields a glycosyltransferase inhibitor within cells. *Nat. Chem. Biol. 7*, 174−181.
(25) Borodkin, V. S., Schimpl, M., Gundogdu, M., Rafie, K., Dorfmueller, H. C., Robinson, D. A., and van Aalten, D. M. (2014) Bisubstrate UDP-peptide conjugates as human O-GlcNAc transferase inhibitors. *Biochem. J. 457*, 497−502.
(26) Bernardes, G. J. L., Grayson, E. J., Thompson, S., Chalker, J. M., Errey, J. C., El Oualid, F., Claridge, T. D. W., and Davis, B. G. (2008) From disulfide- to thioether-linked glycoproteins. *Angew. Chem., Int. Ed. 47*, 2244−2247.
(27) Wittrock, S., Becker, T., and Kunz, H. (2007) Synthetic vaccines of tumor-associated glycopeptide antigens by immune-compatible thioether linkage to bovine serum albumin. *Angew. Chem., Int. Ed. 46*, 5226−5230.
(28) Floyd, N., Vijayakrishnan, B., Koeppe, A. R., and Davis, B. G. (2009) Thiyl Glycosylation of Olefinic Proteins: S-Linked Glycoconjugate Synthesis. *Angew. Chem., Int. Ed. 48*, 7798−7802.
(29) Dondoni, A. (2008) The Emergence of Thiol-Ene Coupling as a Click Process for Materials and Bioorganic Chemistry. *Angew. Chem., Int. Ed. 47*, 8995−8997.
(30) Hoyle, C. E., and Bowman, C. N. (2010) Thiol-Ene Click Chemistry. *Angew. Chem., Int. Ed. 49*, 1540−1573.
(31) Bogachev, V. S. (1996) Synthesis of deoxynucleoside 5′-triphosphates using trifluoroacetic anhydride as an activating reagent. *Bioorganicheskaya Khimiya 22*, 699−705.
(32) Marlow, A. L., and Kiessling, L. L. (2001) Improved chemical synthesis of UDP-galactofuranose. *Org. Lett. 3*, 2517−2519.
(33) Fairbanks, B. D., Schwartz, M. P., Bowman, C. N., and Anseth, K. S. (2009) Photoinitiated polymerization of PEG-diacrylate with lithium phenyl-2,4,6-trimethylbenzoylphosphinate: polymerization rate and cytocompatibility. *Biomaterials 30*, 6702−6707.
(34) Derossi, D., Joliot, A. H., Chassaing, G., and Prochiantz, A. (1994) The third helix of the Antennapedia homeodomain translocates through biological membranes. *J. Biol. Chem. 269*, 10444−10450.
(35) Vivès, E., Brodin, P., and Lebleu, B. (1997) A truncated HIV-1 Tat protein basic domain rapidly translocates through the plasma membrane and accumulates in the cell nucleus. *J. Biol. Chem. 272*, 16010−16017.
(36) Schmidt, N., Mishra, A., Lai, G. H., and Wong, G. C. L. (2010) Arginine-rich cell-penetrating peptides. *FEBS Lett. 584*, 1806−1813.
(37) Langel, Ü. (2015) Cell-Penetrating Peptides: Methods and Protocols, 2nd Edition pp 1−472, Vol. *1324*, DOI: 10.1007/978-1-4939-2806-4.

DOI: 10.1021/acs.bioconjchem.8b00194
Bioconjugate Chem. 2018, 29, 1834−1840

(38) Pathak, S., Alonso, J., Schimpl, M., Rafie, K., Blair, D. E., Borodkin, V. S., Schuttelkopf, A. W., Albarbarawi, O., and van Aalten, D. M. F. (2015) The active site of O-GlcNAc transferase imposes constraints on substrate sequence. *Nat. Struct. Mol. Biol. 22*, 744−U133.

DOI: 10.1021/acs.bioconjchem.8b00194
Bioconjugate Chem. 2018, 29, 1834−1840